Development of Cleavage Fracture Toughness Locus Considering Constraint Effects

Yoon-Suk Chang*, Young-Jin Kim
SAFE Research Centre, School of Mechanical Engineering, Sungkyunkwan University, 300 Chunchun-dong, Jangan-gu, Suwon, Kyonggi-do 440-746, Korea
Ludwig Stumpfrock
Staatliche Materialprufungsanstalt, Universitat Stuttgart, Pfaffenwaldring 32, D-70569 Stuttgart, Germany

In this paper, the higher order terms in the crack tip stress fields are investigated macroscopically for more realistic assessment of structural material behaviors. For reactor pressure vessel material of A533B ferritic steel, effects of crack size and temperature have been evaluated using 3-point SENB specimens through a series of finite element analyses, tensile tests and fracture toughness tests. The T-stress, Q-parameter and q-parameter as well as the K and J-integral are calculated and mutual relationships are investigated also. Based on the evaluation, it has proven that the effect of crack size from standard length ($a/W=0.53$) to shallow length ($a/W=0.11$) is remarkable whilst the effect of temperature from -20℃ to -60℃ is negligible. Finally, the cleavage fracture toughness loci as a function of the promising Q-parameter or q-parameter are developed using specific test results as well as finite element analysis results, which can be applicable for structural integrity evaluation considering constraint effects.

Key Words: Constraint Effect, Two-parameter Approach, Modified Boundary Layer Formulation, T-stress, Q-parameter, q-parameter, Biaxiality Ratio, Cleavage Fracture Toughness Locus

1. Introduction

Since 1960's, fracture mechanics theories have been developed to account for various types of material behaviors and geometric discrepancy. The characterization of crack tip stress and strain fields is essential to the fracture mechanics (Jeon et al., 2003) and, Mode I is a representative one among the three types of basic loading that a crack can experience. In LEFM (Linear Elastic Fracture Mechanics), asymptotic stress and displacement fields of the crack tip described as Eq. (1) and Eq. (2) respectively in which those are expressed using SIF (Stress Intensity Factor) K after ignoring higher order terms. The higher order terms depend on geometry but thought as not significant when comparing with the leading term that is proportional to $1/\sqrt{r}$ (Anderson, 1995).

$$\sigma_{xx}=\frac{K_I}{\sqrt{2\pi r}}\cos\left(\frac{\theta}{2}\right)\left[1-\sin\left(\frac{\theta}{2}\right)\sin\left(\frac{3\theta}{2}\right)\right]$$

$$\sigma_{yy}=\frac{K_I}{\sqrt{2\pi r}}\cos\left(\frac{\theta}{2}\right)\left[1+\sin\left(\frac{\theta}{2}\right)\sin\left(\frac{3\theta}{2}\right)\right] \quad (1)$$

$$\tau_{xy}=\frac{K_I}{2\pi r}\cos\left(\frac{\theta}{2}\right)\sin\left(\frac{\theta}{2}\right)\cos\left(\frac{3\theta}{2}\right)$$

* Corresponding Author,
E-mail : yschang7@skku.edu
TEL : +82-31-290-7459; **FAX** : +82-31-290-5276
SAFE Research Centre, School of Mechanical Engineering, Sungkyunkwan University, 300 Chunchun-dong, Jangan-gu, Suwon, Kyonggi-do 440-746, Korea.
(Manuscript **Received** May 6, 2004; **Revised** September 23, 2004)

$$u_x=\frac{(1+v)K_I}{E}\sqrt{\frac{r}{2\pi}}\cos\left(\frac{\theta}{2}\right)\left[\kappa-1+2\sin^2\left(\frac{\theta}{2}\right)\right]$$
$$u_y=\frac{(1+v)K_I}{E}\sqrt{\frac{r}{2\pi}}\sin\left(\frac{\theta}{2}\right)\left[\kappa+1-2\cos^2\left(\frac{\theta}{2}\right)\right] \quad (2)$$

where, E is a Young's modulus, n is a Poisson's ratio and $\kappa=3-4n$ for plane strain condition.

In EPFM (Elastic-plastic Fracture Mechanics), J-integral can be used to characterize the crack tip conditions instead of K. The stress and strain fields described as Eq. (3) are obtained by applying the appropriate boundary conditions.

$$\sigma_{ij}=\sigma_0\left(\frac{EJ}{\alpha\sigma_0^2 I_n r}\right)^{\frac{1}{n+1}}\tilde{\sigma}_{ij}(n,\theta)$$
$$\varepsilon_{ij}=\frac{\alpha\sigma_0}{E}\left(\frac{EJ}{\alpha\sigma_0^2 I_n r}\right)^{\frac{n}{n+1}}\tilde{\varepsilon}_{ij}(n,\theta) \quad (3)$$

where, σ_0 is a reference stress usually equal to yield strength, $\varepsilon_o=\sigma_0/E$, α is a dimensionless material constant, n is a strain hardening exponent and I_n is an integration constant which depends on n are dimensionless functions of n and θ. Eq. (3) is called the HRR singularity named after Hutchinson, Rice and Rosengren (1968; 1968).

A structure under SSY (Small-Scale Yielding) condition has two singularity-dominated zones; the one in the elastic region where stress varies as $1/\sqrt{r}$ and the other in the plastic zone where stress varies as $r^{-1/(n+1)}$. In reality, however, the singular field does not persist all the way to the crack tip. The large scale yielding near the crack tip causes a blunting which reduces the stress triaxiality locally. The blunted crack tip is a free surface and thus σ_{xx} must vanish at $r=0$. The analysis that leads to the HRR singularity does not consider the effect of the blunted crack tip on the stress fields, nor does it take account of the large strains that are present near the crack tip. This is based on small strain theory that breaks down when strains are greater than 10% (Anderson, 1995).

In this paper, the higher order terms in the crack tip stress fields are investigated for reactor pressure vessel material of A533 ferritic steel. The effects of different crack size and temperature are evaluated using 3-point SENB (Single Edge Notched Bend) specimens through a series of finite element analyses and fracture toughness tests based on macroscopic two-parameter approaches using T-stress, Q-parameter and q-parameter. Thereby cleavage fracture toughness loci are developed for realistic structural integrity evaluation considering constraint effects.

2. Summary of Two-Parameter Approach

2.1 J-T Theory (Williams, 1957; Bilby et al., 1986; Betegon and Hancock, 1991; Hancock et al., 1993; Sumpter, 1993; Kirk and Dodds, 1993)

In a cracked body subject to Mode I loading, the T-stress scales with the applied load. The biaxiality ratio (β) which is a constant for a given geometry and loading mode relates T to K_I and expressed in Eq. (4). For laboratory specimens with K_I solutions, the T-stress is given by Eq. (5).

$$\beta=\frac{T\sqrt{\pi a}}{K_I} \quad (4)$$

$$T=\frac{\beta P}{B\sqrt{\pi a W}}f\left(\frac{a}{W}\right) \quad (5)$$

The J-T theory has been successfully used as a convenient means to investigate and characterize specimen geometry effects on near tip stress triaxiality under conditions of well-contained yielding (Bilby et al., 1986; Betegon and Hancock, 1991). However, this methodology has limitations because the T-stress is an elastic parameter. The T-stress estimated from load through Eq. (5) has little physical meaning under fully plastic condition. It was addressed that J-T theory provides a good practical method of predicting the nature of the higher order terms in FFS (Full Field Solution) (Betegon and Hancock, 1991). The appropriate toughness for real structural defects can be matched against that of test specimens with similar constraint through the use of J-T fracture locus. Therefore, experimental confirmation with J_c is recommended in general.

2.2 J-Q Theory (O'Dowd and Shih, 1991; 1992; O'Dowd et al., 1995; Shih et al., 1991)

In the two-parameter approach using the Q-parameter, the crack tip stress fields are assumed to be

$$\sigma_{ij}=(\sigma_{ij})_{HRR}+Q\sigma_0\delta_{ij} \text{ or } \sigma_{ij}=(\sigma_{ij})_{SSY;T=0}+Q\sigma_0\delta_{ij} \quad (6)$$

where, δ_{ij} is the Kronecker delta. Typically the Q-parameter is defined by

$$Q\equiv\frac{\sigma_{yy}-(\sigma_{yy})_{HRR}}{\sigma_0} \text{ or } Q\equiv\frac{\sigma_{yy}-(\sigma_{yy})_{SSY;T=0}}{\sigma_0} \quad (7)$$

at $\theta=0$ and $r\sigma_0/J=2$

The Q values under SSY condition are available from the relation between Q and the T-stress in which the crack tip is assumed to remain sharp whilst the present analysis is focused on obtaining the Q values under LSY (Large-Scale Yielding) condition. Once T-stress is known, Q-parameter may be determined from the Q-T relationship. The T-stress relates uniquely to the Q-parameter under SSY condition. Within the MBLF (Modified Boundary Layer Formulation), the Q-parameter may depend on the T-stress alone. For a power-law hardening material, there is a one-to-one correspondence between these two parameters as follows (O'Dowd and Shih, 1992):

$$Q_{SSY}=F(T/\sigma_0;\ n) \quad (8)$$

In Eq. (8), the subscript SSY emphasizes that the results are derived from a small scale yielding solution. The F additionally depends on dimensionless combinations of material parameters though which is expected to be weak. This can be translated as a description of near-tip states by J and Q is equivalent to that phrased in terms of K and T since Q-parameter and T-stress are related by Eq. (8), and J and K are related as follows. However, this equivalence does not hold under fully yielded condition.

$$J=\frac{(1-\nu^2)K_I^2}{E} \quad (9)$$

Under SSY condition the J-T and J-Q theories are equivalent. Even though it can be obtained from finite strain formulation also, based on full-field numerical investigations, the T-stress does not adequately quantify the crack tip constraint under LSY condition.

2.3 q-parameter (Clausmeyer et al., 1991; Pavankumar et al., 2001)

As one of the constraint parameters, the multi-axiality quotient (q) is defined as follows:

$$q=\frac{\sigma_e}{\sqrt{3}\ \sigma_m} \quad \text{at } 1\leq r\sigma_0/J\leq 5 \quad (10)$$

where, σ_m is a hydrostatic stress and σ_e is a von Mises effective stress.

The small values of q represent high degree of stress triaxiality according to above definition. The q- and Q-parameters can be used to describe the crack tip constraint conditions in a similar fashion. A relationship between these two parameters was investigated in order to convert from one parameter to the other easily for a specific material (Clausmeyer et al., 1991). The relationship is derived as follows:

$$q=\frac{1}{(mQ+c)\sqrt{3}} \quad \text{at } 1\leq r\sigma_0/J\leq 5 \quad (11)$$

where, $m=\sigma_0/(\sigma_e)_{ref}$, $c=(\sigma_m/\sigma_e)_{ref}$ and ref means HRR or SSY solution. In this paper, regarding the q-parameter determination, the SSY solution is mainly used as the ref.

3. Material Property

3.1 Tensile test data

The constraint effects are most pronounced for low-to-medium strength structural steels operating in the ductile-to-brittle transition region where unstable fracture occurs by the micro-mechanism of transgranular cleavage. In this research, A533B ferritic steel (HSST Plate 14) is used. It is heat treated to achieve an elevated yield strength by approximating that for a typical radiation sensitive RPV (Reactor Pressure Vessel) steel irradiated to a fluence of 1.5×10^{19} n/cm^2 (E>1 MeV). The resulting room temperature yield strengths are in the range of 620~655 MPa.

Table 1 and Fig. 1 show the basic properties and stress-strain curves of the material obtained from uni-axial tensile tests and by extension until strain of unity. A Poisson's ratio of 0.3 is assumed and all of these data that depend on temperatures are used as inputs for corresponding finite element analyses. Also, for engineering application, it may necessary to express the full range tensile test data as a power law relationship. Eq. (12) represents a Ramberg-Osgood (R-O) equation which is widely used for stress-strain data curve fitting.

Table 1 Basic tensile properties of A533B ferritic steel

Temperature (℃)	−20	−40	−60
Young's Modulus (MPa)	217000	220250	223500
Yield Strength (MPa)	657	668	678

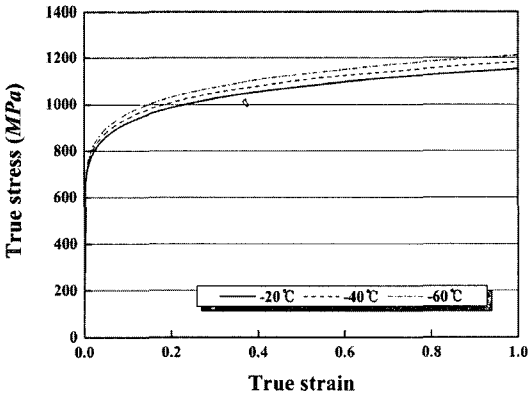

Fig. 1 Stress-strain curves of A533B ferritic steel

$$\frac{\varepsilon}{\varepsilon_0}=\frac{\sigma}{\sigma_0}+\alpha\left(\frac{\sigma}{\sigma_0}\right)^n \tag{12}$$

The temperature-dependent power law relationships of material were derived using Eq. (12) and experimental tensile test data. Resulting values of R-O parameters shown in Table 2 are used for HRR solution.

3.2 Fracture toughness test data

In this research, total 28 fracture toughness tests have been carried out using SENB specimens with 25 mm-thickness. Table 3 describes the representative dimensions used in the tests and utilized for FE (Finite Element) model generation. Table 4 summarizes the minimum ($J_{c,\min}$) and maximum ($J_{c,\max}$) fracture toughness test data of the material at each temperature according to ASTM E1820-99 (1999). As shown in the table, even though the fracture toughnesses of low constraint shallow cracked specimens are higher than the fracture toughnesses of high constraint standard cracked specimens, there are large scatters since the tests have been performed in the ductile-to-brittle transition region.

Table 2 Ramberg-Osgood parameters of A533B ferritic steel

Temperature (℃)	ε_0	α	n
−20	0.003028	0.425	12.337
−40	0.003033	0.414	12.214
−60	0.003034	0.424	11.942

Table 3 SENB specimen dimensions used in test (mm)

Geometry	Thickness (B)	Net Thickness (B_{net})	Width (W)	Length (L)	Span (S)	Initial Crack Length (a_0)
Shallow Crack	24.94	19.89	24.95	125	100	2.74
Standard Crack	25.00	19.97	24.89	125	100	13.27

Table 4 Fracture toughness test data of A533B ferritic steel

Temperature (℃)	Shallow Crack		Standard Crack	
	$J_{c,\min.}$(kN/m)	$J_{c,\max.}$(kN/m)	$J_{c,\min.}$(kN/m)	$J_{c,\max.}$(kN/m)
−20	15	263	48	247
−40	64	374	20	144
−60	22	162	29	49

4. Numerical Analysis

4.1 HRR solution

The reference HRR solutions, $(\sigma_{ij})_{HRR}$, were obtained from the crack tip stress and relevant R-O parameters using Eq. (3). Fig. 2 shows temperature dependence of the HRR solutions in which the reference non-dimensional tangential stresses are illustrated along the non-dimensional distance.

4.2 Boundary layer formulation

The finite element analyses were carried out by ABAQUS Code (2001) with focused meshes shown in Fig. 3. The mesh contains 320 8-noded biquadratic plane strain quadrilateral elements consisting of 20 rings and 16 elements concentric with the crack tip. McMeeking suggests that if the CTOD (Crack-Tip Opening Displacement) after deformation is at least 5 times the initial value, the results should not be affected by the initial blunt notch (McMeeking and Parks, 1989). The crack tip is modeled to having very small finite root radius of 1×10^{-5} mm in order to incorporate a blunting region. During loading, the crack tips were blunted to maximum openings between 10 and 15 times their undeformed openings to assure that the initial notch radius would not affect on the results. The crack tip was defined by 33 nodes, which were regularly spaced on a quarter-circle shaped line, and the mesh is regarded as fine to fulfill the condition suggested by other researchers (Varias et al., 1991).

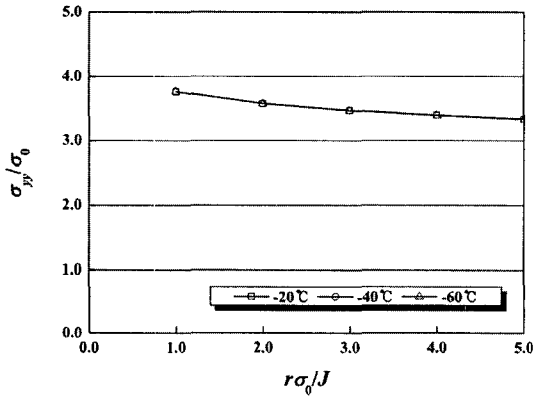

Fig. 2 Temperature dependence of reference non-dimensional tangential stress directly ahead of the crack tip from HRR solution

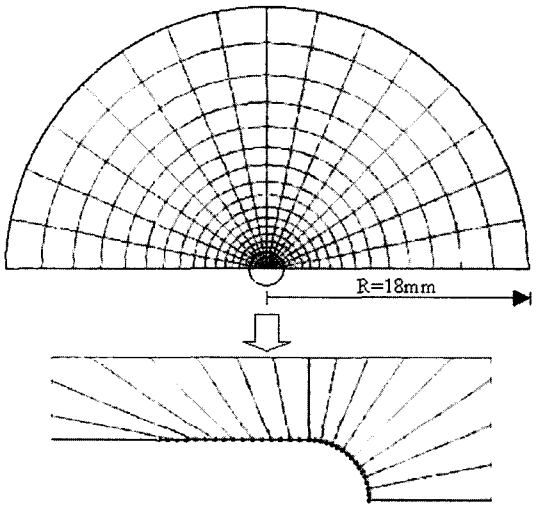

Fig. 3 FE mesh for BLF

The displacement boundary conditions in Eq. (2) were imposed on the outer boundary corresponding to the displacements associated with a K field. In order to determine the specific boundary layer solutions of material, the incremental plasticity option were used based on the stress-strain curves shown in Fig. 1. Table 5 summarizes the boundary layer solutions directly ahead of the crack tip. The validities of the boundary layer solutions are checked in Fig. 4 through comparison of the non-dimensional tangential stresses

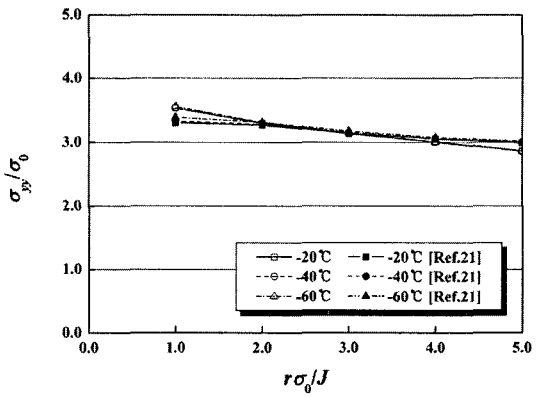

Fig. 4 Comparison of non-dimensional tangential stresses directly ahead of the crack tip from BLF with reference results

Table 5 Boundary layer solutions, σ_{yy} (MPa), of A533B ferritic steel ($\theta=0°$)

Temperature (℃)	$r\sigma_0/J=1$	$r\sigma_0/J=2$	$r\sigma_0/J=3$	$r\sigma_0/J=4$	$r\sigma_0/J=5$
−20	2320.2	2162.3	2059.2	1971.5	1879.8
−40	2365.9	2203.3	2096.9	2006.7	1912.5
−60	2410.3	2242.3	2132.9	2040.1	1943.4

Table 6 T-stress (MPa) of shallow and standard cracked specimens

Temperature(℃)	Shallow cracked specimen ($a/W=0.110$)	Standard cracked specimen ($a/W=0.533$)
−20	−497.5	287.7
−40	−505.8	292.5
−60	−513.4	296.9

directly ahead of crack tip and corresponding reference results (O'Dowd, 1992; Dodds et al., 1992).

4.3 Modified boundary layer formulation

Several relationships to estimate the biaxiality ratios, β, have been proposed for different crack length to width (a/W) ratios. Sham et al. suggested tabulated values (Sumpter, 1993). The β-a/W relationships were also suggested by Leevers et al.(1982), Anderson (1995) and Kirk et al.(1993) respectively. In this paper, the β values by Kirk et al. were adopted since those were presented recently as a fitting equation and there were no big differences to the other values until $a/W=0.4$. Using the β values, specimen geometries and Eq. (4), the T-stresses of shallow and standard cracked specimens were determined. Table 6 summarizes the results for different crack sizes and temperatures.

The reference solutions, $(\sigma_{ij})_{SSY,T\neq0}$, were obtained from the crack tip stress field through modified boundary layer formulation. The finite element model and analyses method were same with the boundary layer formulation except the displacement boundary conditions. The previous displacement boundary conditions in Eq. (2) were modified as Eq. (13) that imposed on the outer boundary corresponding to the displacements associated with K field plus the displacements due to the T-stress (Al-Ani and Hancock, 1991). In other words, the elastic-plastic crack

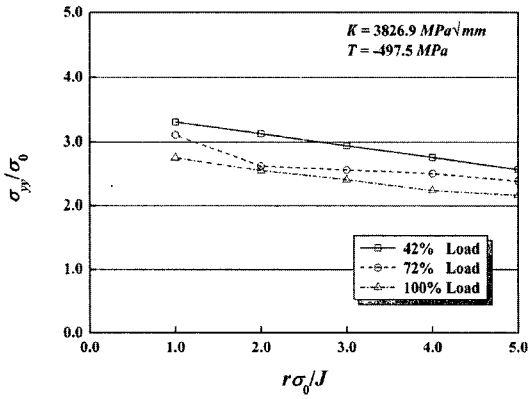

Fig. 5 Applied load dependence of reference non-dimensional tangential stress directly ahead of the crack tip from MBLF at −20℃ (shallow cracked specimens)

tip fields in SSY condition were generated by applying displacements consistent with the first two terms of the linear elastic crack tip fields to a circular region containing an edge crack. In order to ensure that the SSY assumption is satisfied, the FE mesh was modeled sufficiently large.

$$u_x=\frac{(1+v)K_I}{E}\sqrt{\frac{r}{2\pi}}\cos\left(\frac{\theta}{2}\right)\left[\kappa-1+2\sin^2\left(\frac{\theta}{2}\right)\right]+(1-v^2)\frac{\beta}{E\sqrt{\pi a}}K_I r\cos\theta$$

$$u_y=\frac{(1+v)K_I}{E}\sqrt{\frac{r}{2\pi}}\sin\left(\frac{\theta}{2}\right)\left[\kappa+1-2\cos^2\left(\frac{\theta}{2}\right)\right]-v(1+v)\frac{\beta}{E\sqrt{\pi a}}K_I r\sin\theta \tag{13}$$

Table 7 Modified boundary layer solutions, σ_{yy} (MPa), of A533B ferritic steel ($\theta=0°$)

Identification	$r\sigma_0/J=1$	$r\sigma_0/J=2$	$r\sigma_0/J=3$	$r\sigma_0/J=4$	$r\sigma_0/J=5$
−20℃ Shallow	2008.8	1820.2	1735.6	1645.1	1560.8
−40℃, Shallow	2050.4	1856.2	1768.8	1675.7	1588.8
−60℃, Shallow	2091.4	1890.7	1800.6	1704.9	1615.7
−20℃, Standard	2415.1	2256.7	2154.6	2068.9	1979.2
−40℃, Standard	2463.0	2299.5	2194.1	2105.9	2013.5
−60℃, Standard	2509.3	2340.2	2231.7	2140.8	2046.0

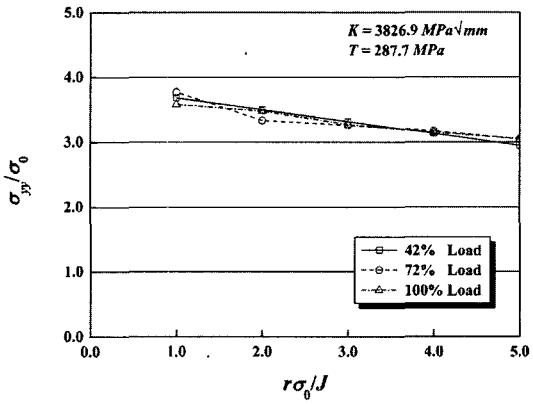

Fig. 6 Applied load dependence of reference non-dimensional tangential stress directly ahead of the crack tip from MBLF at −20℃ (standard cracked specimens)

Figures 5 and 6 show load dependence of the boundary layer solutions for shallow and standard cracked specimens at −20℃. As shown in the figures, the solutions for shallow cracked specimen were dependent on the applied loads though the solutions for standard cracked specimen were little dependent on the loads. These phenomena were occurred also for other temperatures and considered due to the different constraint conditions of both specimen types.

Table 7 summarizes the modified boundary layer solutions directly ahead of the crack tip using mean value solutions. For verification, the J-integrals which were determined by ABAQUS and from the K and T-stress components were compared. In this comparison, the loading conditions of $T=0$ state were determined by $\beta=0$ while the loading conditions of $T\neq 0$ state were determined by $\beta=-0.381$ for shallow cracked specimens and $\beta=0.485$ for standard cracked specimens respectively. Also, the T-stresses which have been determined from ABAQUS directly and Eq. (13) were compared. Even though the comparison results were omitted due to the lack of space, the values of J-integrals and T-stresses are same in both cases.

4.4 T-stress calculation

The elastic T-stresses for both shallow and standard cracked SENB specimens were obtained from a series of elastic finite element analyses whilst the corresponding J-integrals were obtained from elastic-plastic finite element analyses since the T-stress does not affect the J-integral (or K_I). The loading conditions in Eq. (5) were imposed corresponding to the loads associated with K field plus the loads due to the T-stress. The relation between the T-stress and applied load for an SENB specimen is as follows (Kirk et al.,1993):

$$T=1.5\frac{PS}{BW^2}\beta(a/W)\left[1.99-\frac{a}{W}\left(1-\frac{a}{W}\right)\left[2.15-3.93\frac{a}{W}+2.7\left(\frac{a}{W}\right)^2\right]\Big/\sqrt{\pi}\left(1+2\frac{a}{W}\right)\left(1-\frac{a}{W}\right)^{1.5}\right] \quad (14)$$

where, $\beta(a/W)=0.462+0.461\left(\frac{a}{W}\right)+2.47\left(\frac{a}{W}\right)^2$ for $0.025\leq\frac{a}{W}\leq 0.90$.

The typical FE models used for SENB specimens consist of 403 and 460 8-noded biquadratic plane strain quadrilateral elements for shallow cracked model and standard cracked model respectively. The load was applied by distributing tractions over two points to eliminate the local singularity effects caused by a concentrated nodal load. All of the analyses data were retrieved at node points instead of integration points for

Table 8 Biaxiality ratios of SENB specimen that loaded by traction

a/W	0.05	0.15	0.25	0.391	0.50	0.70	0.90
Biaxiality ratio (β)	−0.415	−0.296	−0.178	−0.006	0.137	0.410	1.180

convenient post-processing since there were no remarkable differences in the results, e.g. load and displacement, between node point data and integration point data.

The T-stresses which were determined from ABAQUS directly and Eq. (14) were compared for verification. However, there were differences, especially for the case of positive T-stress. This phenomenon did not occur in the modified boundary layer formulation and it may due to the different biaxiality parameters. In order to resolve the discrepancies, additional review and finite element analyses have been carried out. Kirk and Dodds performed a study to predict size effects on cleavage fracture toughness for several types of specimens that loaded by traction or displacement in which they obtained biaxiality ratios from boundary collocation method (Kirk and Dodds, 1993). Table 8 shows the biaxiality ratios of SENB specimens loaded by traction, which are different with the $\beta(a/W)$ shown in Eq. (14). Therefore, after determining the new biaxiality ratios for traction, a series of elastic finite element analyses have been performed by applying new loads to recalculate the T-stresses for both shallow and standard cracked SENB specimens. The T-stresses which have been determined from ABAQUS directly and Eq. (14) combined with the β values from Table 8 are almost same.

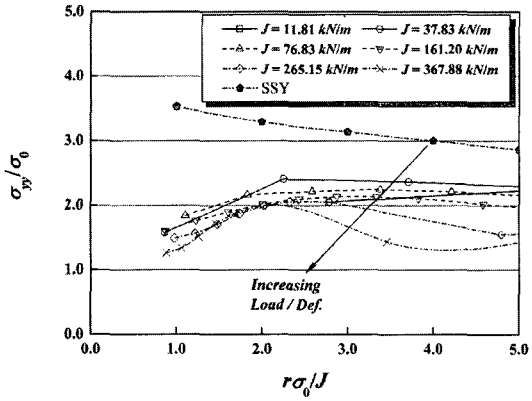

Fig. 7 $\sigma_{yy}/\sigma_0 - r\sigma_0/J$ curves of shallow cracked specimen at −20℃

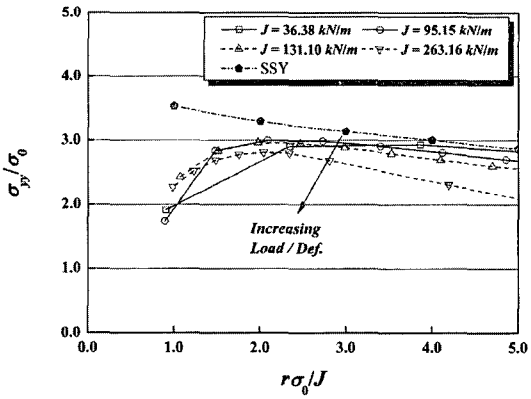

Fig. 8 $\sigma_{yy}/\sigma_0 - r\sigma_0/J$ curves of standard cracked specimen at −20℃

4.5 Q-parameter calculation

The full field solutions for both shallow and standard cracked SENB specimens were obtained from a series of elastic-plastic finite element analyses adopting incremental plasticity option. The geometries of model were same with the elastic T-stress analyses model except for the blunted region, and in which displacement-controlled analyses were carried out.

Figures 7 and 8 show the relationship between non-dimensional stress (σ_{yy}/σ_0) and non-dimensional distance ($r\sigma_0/J$) according to increasing load. Using these data and Eq. (7), the Q-parameters were determined in the region of $1 \leq r\sigma_0/J \leq 5$. The results will be discussed in Chapter 5.

4.6 q-parameter calculation

The full field solutions for both shallow and standard cracked SENB specimens were obtained from a series of elastic-plastic finite element analyses. The model geometries were same with the Q-parameter analyses and displacement-controlled analyses were carried out also.

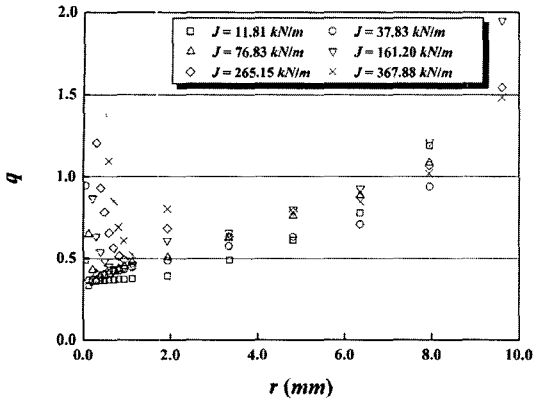

Fig. 9 q-r curves of shallow cracked specimen at −20℃

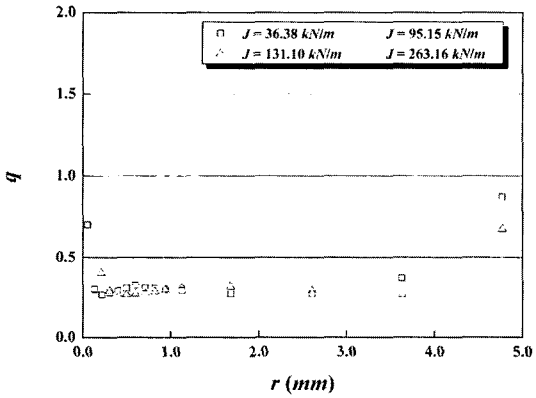

Fig. 10 q-r curves of standard cracked specimen at −20℃

The q-parameters were determined from finite element analyses data and Eq. (10) in the region of $1 \leq r\sigma_0/J \leq 5$. Figures 9 and 10 show the q-parameters at $r\sigma_0/J=2$ along the distance from the crack tip. The q-parameters were decreased at vicinity of the crack tip and increased after some distance from the crack tip.

5. Constraint Effect Evaluation

5.1 J-T analysis

Two types of J-T analyses have been performed based on the modified boundary layer solutions; in the first analyses all the non-dimensional stresses dependent on varying applied loads were used which is a general approach, in the second analyses just the mean values of non-dimensional stresses were used. Figure 11 shows the non-dimensional stresses against non-dimensional T-stresses at $r\sigma_0/J=2$ and 5 according to varying applied loads. Fig. 12 shows the comparison of the non-dimensional parameters

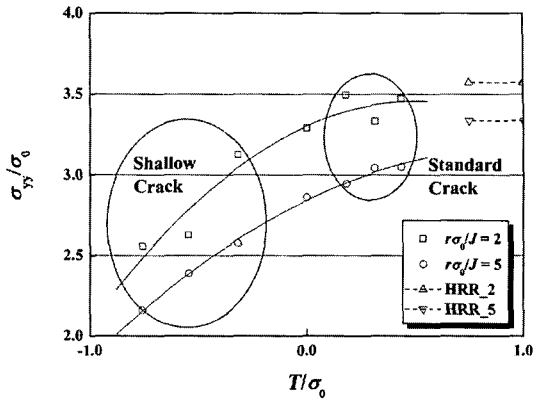

(a) At-20℃

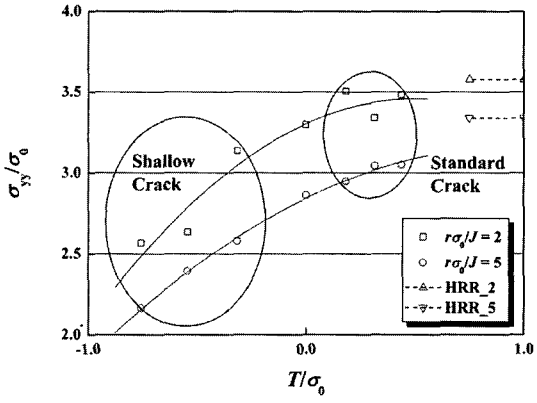

(b) At-40℃

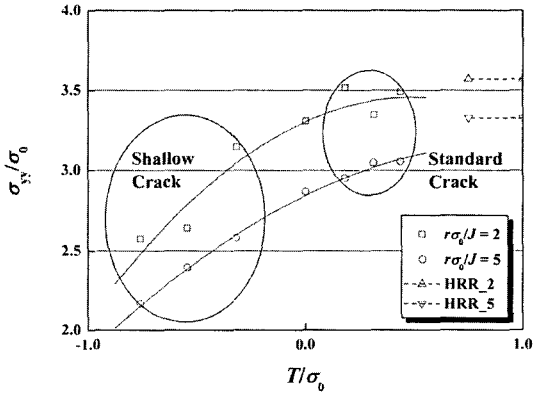

(c) At-60℃

Fig. 11 $\sigma_{yy}/\sigma_0 - T/\sigma_0$ curves from varying loads of MBLF

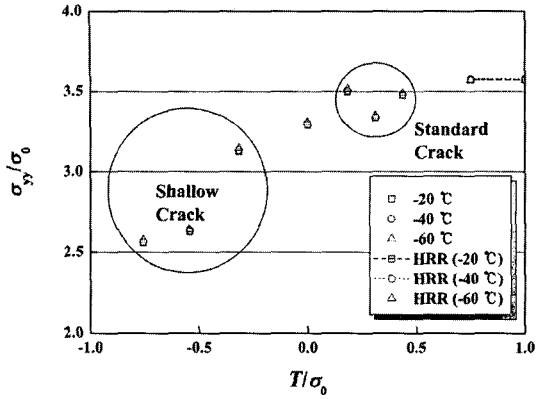

Fig. 12 Comparison of $\sigma_{yy}/\sigma_0 - T/\sigma_0$ curves at $r\sigma_0/J=2$ from varying loads of MBLF

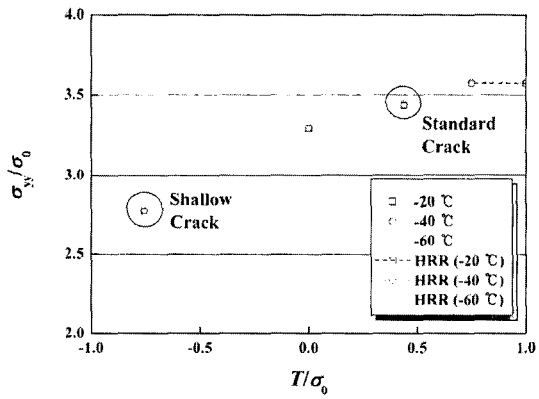

Fig. 13 Comparison of $\sigma_{yy}/\sigma_0 - T/\sigma_0$ curves at $r\sigma_0/J=2$ from mean values of MBLF

at $r\sigma_0/J=2$ according to varying loads to check the temperature effects. Also, the mean values of non-dimensional stresses against non-dimensional T-stresses at $r\sigma_0/J=2$ were presented in Fig. 13. As shown in the Figs. 12 and 13, even though there were no significant influences of temperatures, the non-dimensional stresses of shallow cracked specimens were strongly dependent on load increments while the ones of standard cracked specimens were weakly influenced by the loads. On the other hand, Fig. 14 shows the distribution of von Mises stresses at -20℃ in which shape and size of crack tip stress fields were varied with decreasing T-stress, i.e., showed the loss of constraint behavior. Similar trends were also observed at −40℃ and −60℃.

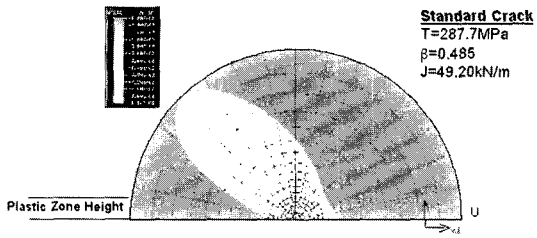

(a) $T/\sigma_0=0.438$ condition

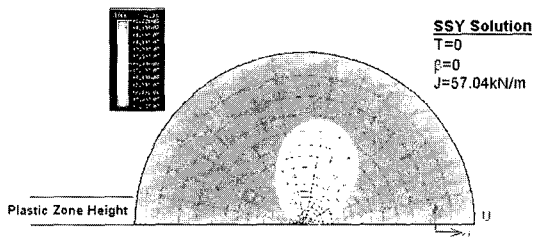

(b) $T/\sigma_0=0$ condition

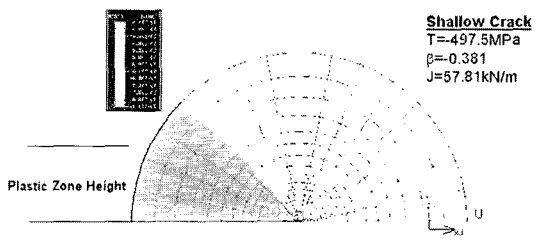

(c) $T/\sigma_0=-0.757$ condition

Fig. 14 Distribution of von Mises stress from varying T-stresses at −20℃

J-T analyses have been carried out based on the full field solutions. For the analyses, the T-stresses determined by ABAQUS with the β values from Table 8 were used since, as mentioned in Chapter 4, the two T-stresses determined by ABAQUS and Eq. (14) combined with the β values from Table 8 were almost same. The non-dimensional stresses against non-dimensional T-stresses at $r\sigma_0/J=2$ from the full field solutions with the modified boundary layer solutions were compared. As the applied load increases, the full field solutions were depart from the modified boundary layer solutions such as at $T/\sigma_0=-0.5$ for the shallow cracked specimens and at $T/\sigma_0=0.3$ for the standard cracked specimen. The reason was considered that the elastic solution, upon which the T-stress is based, is an asymptotic condition which is increasingly violated as plastic flow progresses

beyond well-contained yielding (O'Dowd and Shih, 1991). The plastic flow under LSY relieves stresses at the crack tip and drops them below the modified boundary layer solutions. In addition, it was anticipated that the zero-load condition for all the SENB specimens would occur at $T=0$ and $\sigma_{yy}/\sigma_0=3.3$. However, the corresponding results near this initial point could not obtained since mesh refinement limits the ability to accurately resolve near the crack tip stresses below a certain load (Kirk and Dodds, 1993).

5.2 J-Q analysis

Three types of J-Q analyses have been performed; the first one was using displacement-controlled full field solution with HRR solution, the second one was using displacement-controlled full field solution with boundary layer solution and the last one was using load-controlled full field solution with boundary layer solution. As the representative one, Fig. 15 shows J-Q analyses results based on the HRR solution in which the Q-parameters were compared with J-integral as well as non-dimensional distances such as $\log(J/(b\sigma_0))$ and $J/(a\sigma_0)$.

As shown in the figure and the omitted results based on the boundary layer solutions, in general, both the shallow and standard cracked SENB specimens exhibit loss of constraint in accordance with the increasing load. The levels of loss of constraints were higher for shallow cracked specimens than standard cracked specimens while the effect of temperature was not severe. The J-Q analyses results based on the HRR solution and boundary layer solution showed similar trends each other even though the levels of loss of constraint were higher when adopting the HRR solution. Also, the J-Q analyses results based on load-controlled full field solution showed similar trends even though somewhat different behavior in the level of constraint were observed when comparing with the two displacement-controlled analyses results.

5.3 q-Q relationship

The Q-parameters obtained in section 5.2 using tangential stress can be determined also using hydrostatic stress. For the q- and Q-parameters correlation based on Eq. (11), the reference von Mises stress and hydrostatic stresses were calculated previously. A series of finite element analyses were carried out and, as a res-

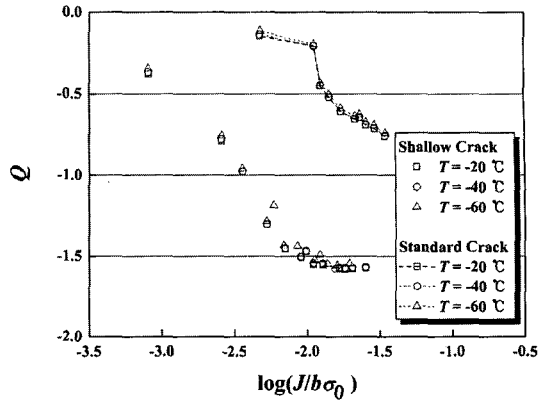

(a) Q-$\log(J/b\sigma_0)$ curves

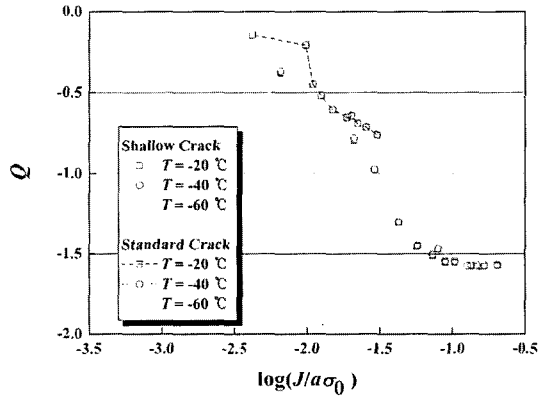

(b) Q-$\log(J/a\sigma_0)$ curves

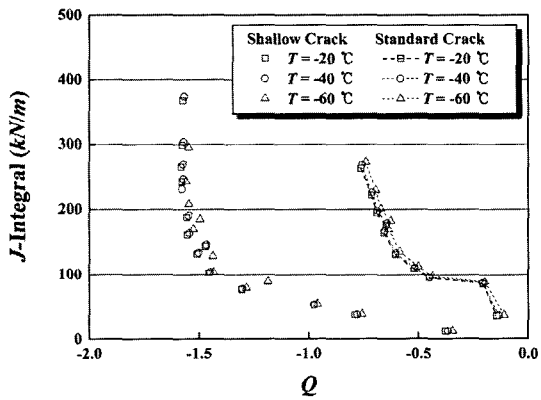

(c) J-Q curves

Fig. 15 Curves based on displacement-controlled FFS combined with HRR solution

Table 9 Variables of Eq. (11) for A533B ferritic steel

Temperature (℃)	$(\sigma_m)_{ref}$, MPa	$(\sigma_e)_{ref}$, MPa	m	c
−20	1698.4	699.0	0.9400	2.4299
−40	1731.3	711.2	0.9392	2.4342
−60	1762.7	722.6	0.9383	2.4394

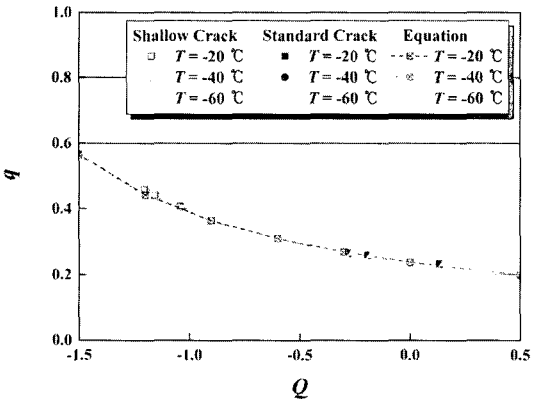

Fig. 16 q-Q relationship using tangential stress

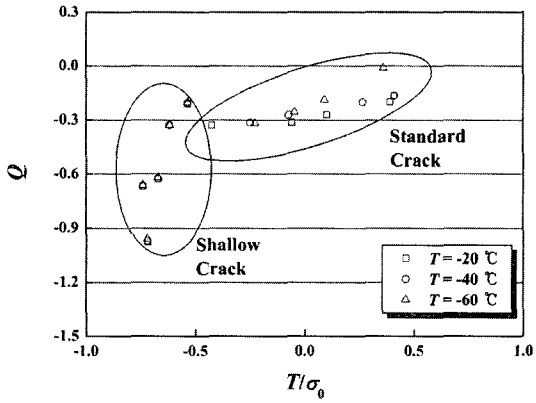

Fig. 17 Q-T/σ_0 curves using T-stress from MBLF

ult, corresponding variables have been derived. Table 9 summarizes the distribution of reference stresses for A533B ferritic steel.

In order to verify the applicability of Eq. (11), the q-Q relationships using both tangential and hydrostatic stresses were checked based on variables in Table 9. As shown in Fig. 16, as the one using the tangential stress at $r\sigma_0/J=2$, good results were obtained as q-Q relationships. Also, there were little differences of the two types of stresses used for the Q-parameter calculation.

5.4 Q-T relationship

For Q-parameter and T-stress correlation, the Q-parameters from the elastic-plastic load-controlled full field solutions were utilized combined with the elastic T-stresses obtained from both the modified boundary layer solutions and full field solutions. In case of utilizing the T-stress from modified boundary layer solutions, the Q-T relationships were determined based on curve fitted J-T equations. Figure 17 shows the relationships between Q-parameters and non-dimensional T-stresses for shallow and standard cracked specimens. As shown in the figure, under limited J-integral ranges, it seems possible to derive a unified relationship. In case of utilizing elastic full field solutions, the T-stresses that determined by ABAQUS with the β values from Table 8 were used. However, similar to the previous J-T analyses results, the standard cracked SENB specimens exhibit different behaviors to the corresponding modified boundary layer solution and it can not possible to derive an unified relationship.

O'Dowd and Shih have performed various analyses based on a small strain J_2 flow theory. In these analyses they proposed a Q-T relationship as a following polynomial expression (O'Dowd and Shih, 1992).

$$Q=a_1\left(\frac{T}{\sigma_0}\right)+a_2\left(\frac{T}{\sigma_0}\right)^2+a_3\left(\frac{T}{\sigma_0}\right)^3 \qquad (15)$$

where, a_1, a_2 and a_3 are least square fitting constants and which values are listed in Table 10 for several n values.

In order to check the validity and applicability of Eq. (15) and corresponding constants, the actual Q values and the predicted ones by the T-stress with ASTM limit $(25J/\sigma_0)$ for valid J_{IC} test are compared. For shallow crack-

Table 10 Fitting constants for Q-T relationship (O' Dowd and Shih, 1992)

n	a_1	a_2	a_3
3	0.6438	−0.1864	−0.0448
5	0.7639	−0.3219	−0.0906
10	0.7594	−0.5221	0.0
20	0.7438	−0.6673	0.1078
∞	0.6567	−0.8820	0.3275

ed specimen, T-stress estimates the stress triaxiality reasonably at low loading condition and deviate according to the load increment. The reason of deviation is considered that the T-stress loses its meaning for LSY. Under this condition, the crack tip stresses and strains are no longer increase in proportion to one another with amplitude governed by J alone. At these high deformation levels, equivalence of J-integrals between different cracked geometries does not insure identical crack tip stress and strain fields (Kirk and Dodds, 1993). However, for standard cracked specimen, Eq. (15) fails to predict the stress triaxiality even though at low loading condition.

Nevertheless the promising previous results (Betegon and Hancock, 1991; O'Dowd and Shih, 1992), according to the above evaluations, the Q-T relationship seems not have general applicability since the T-stress is defined from asymptotic elastic solution which is increasingly violated as plastic flow progresses beyond well-contained yielding. Therefore, based on the limited analyses results on this report, the application of Q-T relationship is not recommended.

6. Cleavage Fracture Toughness Locus

6.1 Crack size effect

In order to examine the crack size effects, the modified boundary layer analyses results have been synthesized with the HRR and boundary layer solutions, i.e., $T=0$ condition. Fig. 18 shows the variation of non-dimensional stresses along non-dimensional distances for both shallow and standard cracked specimens at −20℃.

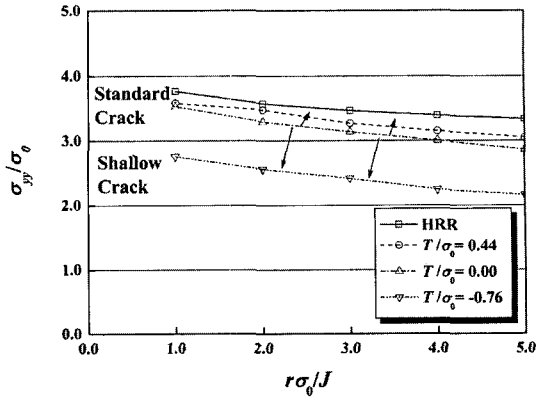

Fig. 18 Variation of non-dimensional stress due to T-stress at −20℃

The non-dimensional stresses with a positive T-stress were somewhat increased with deformation until the data closely approximate to the HRR solutions. The non-dimensional stresses with a negative T-stress were initially close to the $T=0$ condition but significantly decreased with deformation. Therefore, in case of negative T-stress, i.e., for shallow cracked specimen, it will be necessary to consider the loss of constraint effects when performing structural integrity evaluation. Also, similar trends were observed at −40℃ and −60℃.

Figures 19 and 20 show the variation of full field non-dimensional stresses along non-dimensional distances at −60℃ for shallow and standard cracked specimens respectively. As shown in the figures, two types of specimens behaved different manners due to different constraint conditions. For shallow cracked specimen, even at the low loading conditions, the non-dimensional stresses fell significantly below the HRR and boundary layer solutions. Meanwhile, for standard cracked specimen, the non-dimensional stresses at low loading conditions were similar to the boundary layer solution and fell below according to load increment. Similar trends were observed at −20℃ and −40℃.

6.2 Temperature effect

As shown in Fig. 1, the stress-strain curves of A533B ferritic steel vary with test temperatures. The stress-strain curves and yield strengths were

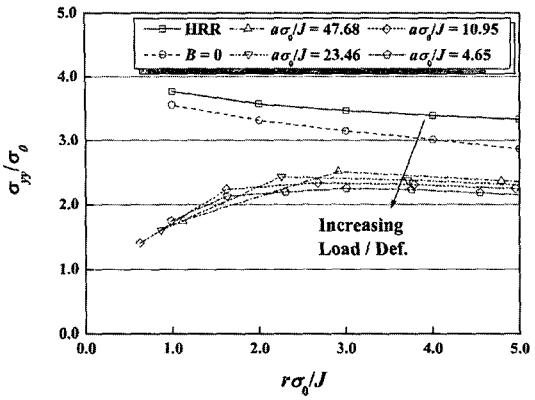

Fig. 19 Variation of full field non-dimensional stress for shallow cracked specimen at −60℃

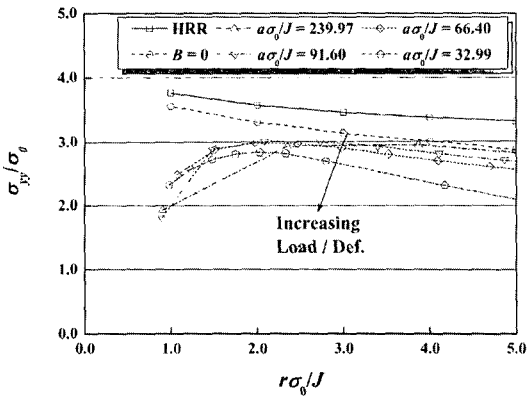

Fig. 20 Variation of full field non-dimensional stress for standard cracked specimen at −60℃

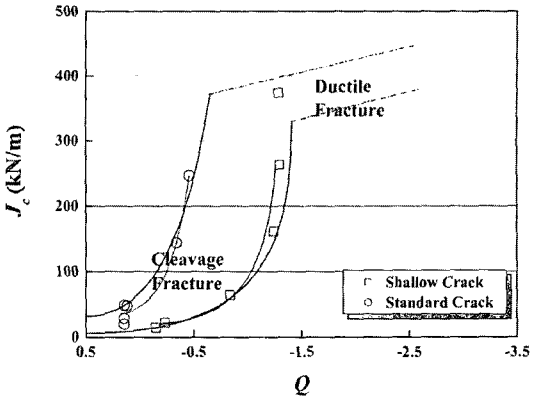

Fig. 21 Cleavage fracture toughness locus based on Q-parameter of A533B ferritic steel

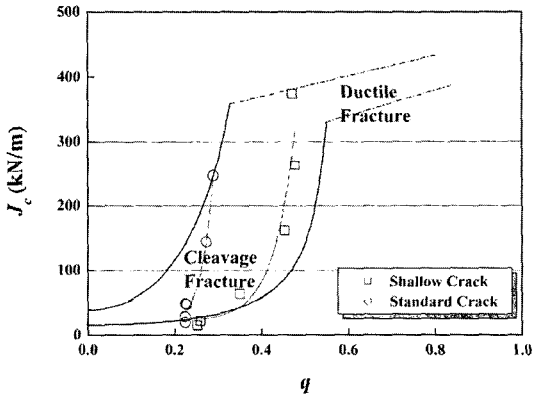

Fig. 22 Cleavage fracture toughness locus based on q-parameter of A533B ferritic steel

higher at lower temperatures and these differences brought on different tangential stresses directly ahead of the crack tip and J-integrals. However, after normalizing with corresponding yield strengths, the differences were vanished and thereafter unique results have been derived. Therefore, numerical analyses point of view, it seems that there are little effect of test temperatures.

6.3 Cleavage fracture toughness locus

The constraint effect evaluation results provide the quantitative framework to characterize a material's fracture resistance for different crack tip stress triaxialities. The numerical analyses results combined with the minimum and maximum critical fracture toughnesses from experiments can be utilized in engineering application. The J_c-Q curve of A533B ferritic steel, which represents insignificant effects of temperature. Thereby, a cleavage fracture toughness locus based on Q-parameter has been obtained in Fig. 21 using all temperature range data. The cleavage fracture toughness locus was divided by two distinct segments since measured toughness values exhibited large scatter and which can be used to define bands for brittle failure.

As discussed in Chapter 5.3, the q- and Q-parameters have good relationship over full temperature ranges. Based on these relationships, i.e., using Eq. (11) and Table 9, J_c-q curve of A533B ferritic steel has been determined. Since

this figure shows also insignificant effects of temperature like J_c-Q curve, a cleavage fracture toughness locus based on q-parameter has been obtained in Fig. 22 using all temperature range data.

In addition, the current cleavage fracture toughness loci that obtained from SENB specimens only can be elaborate by incorporating other geometries and loading conditions. The cleavage fracture toughness locus based on T-stress is not illustrated since the T-stress solution was increasingly violated as plastic flow progresses beyond well-contained yielding.

7. Conclusion

In this paper, for A533B ferritic steel, effects of different crack size (shallow and standard crack size) and temperature (−20, −40 and −60℃) were evaluated using 3-point SENB specimens through a series of finite element analyses, tensile tests and fracture toughness tests. The T-stress, Q-parameter, q-parameter as well as the traditional K and J-integral were determined and thereby mutual relationships have been investigated. The key methods, results and findings are as follows:

(1) The reference SSY solutions $[(\sigma_{ij})_{SSY,T\neq 0}]$ from boundary layer formulations as well as HRR solutions $[(\sigma_{ij})_{HRR}]$ from HRR singularity and Ramberg-Osgood parameters were obtained. In general, the SSY solutions are slightly lower than the HRR solutions since it considered the actual stress-strain relationships.

(2) J-T analyses results based on the modified boundary layer solutions showed crack size dependent trends while there were little dependence on temperatures. Regarding the full field J-T analyses, as the applied load increases, the solutions were depart from the modified boundary layer solutions such as at $T/\sigma_0=-0.5$ for the shallow cracked specimens and at $T/\sigma_0=0.3$ for the standard cracked specimen. The reason was due to a plastic flow under large scale yielding that relieves stresses at the crack tip and drops them below the modified boundary layer solutions.

(3) J-Q analyses have been performed. In general, both the shallow and standard cracked SENB specimens exhibit loss of constraint according to the increasing loads. J-Q fields existed over the entire range of plastic yielding. The levels of loss of constraints were higher for shallow cracked specimens while the effect of temperature was not severe.

(4) There was good relationship between Q-parameter and q-parameter. Therefore, if know the one of the two parameters, it is possible to translate to the other parameter easily.

(5) Numerical analyses results combined with the minimum and maximum fracture toughness values from experiments were utilized for development of the cleavage fracture toughness loci. The J_c-Q or J_c-q curves can be utilized for engineering application considering the constraint effects conveniently.

Acknowledgment

The authors are grateful for the support provided by a grant from MPA at the Stuttgart University and Safety and Structural Integrity Research Centre at the Sungkyunkwan University.

References

ASTM, 1999, "Standard Test Method for Measurement of Fracture Toughness," *ASTM E1820-99*, pp. 972~1005.

Al-Ani, A. M. and Hancock, J. W., 1991, "J-Dominance of Short Cracks in Tension and Bending," *J. of the Mechanics and Physics of Solids*, Vol. 39, No. 1, pp. 23~43.

Anderson, T. L., 1995, "Fracture Mechanics — Fundamentals and Application," CRC Press.

Betegon, C. and Hancock, J. W., 1991, "Two Parameter Characterization of Elastic-Plastic Crack Tip Fields," *J. of Applied Mechanics*, Vol. 58, pp. 104~110.

Bilby, B. A. et al., 1986, "A Finite Element Investigation of the Effect of Specimen Geometry on the Fields of Stress and Strain at the Tips of

Stationary Cracks," *Size Effects in Fracture, Institute of Mechanical Engineers*, pp. 37~46.

Clausmeyer, H., Kussmaul, K. and Roos, E., 1991, "Influence of Stress State on the Failure Behaviour of Cracked Components Made of Steel," *J. of Applied Mechanics*, Vol. 44, No. 2, pp. 77~92.

Dodds, R. H. Jr. and Shih, C. F., 1992, "Continuum and Micro-Mechanics Treatment of Constraint in Fracture," *IAEA/CSNI Specialist's Meeting on Fracture Mechanics Verification by Large Scale Testing*.

HKS, ABAQUS Version 5.8 & Version 6.2.

Hancock, J. W. et al., 1993, "Constraint and Toughness Parameterized by T," Constraint Effects in Fracture, *ASTM STP 1171*, pp. 21~40.

Hutchinson, J. W., 1968, "Singular Behavior at the End of a Tensile Crack Tip in a Hardening Material," *J. of the Mechanics and Physics of Solids*, Vol. 16, pp. 13~31.

Jeon, I. S., Lee, Y. W. and Im, S. Y., 2003, "Higher Order Eigenfields in Mode II Cracks Under Elastic-Plastic Deformation," *KSME International Journal*, Vol. 17, No. 2, pp. 254~268.

Kirk, M. T. and Dodds, R. H. Jr., 1993, "Approximate Techniques for Predicting Size Effects on Cleavage Fracture Toughness (J_c)," *NUREG/CR-5970*.

Kirk, M. T., Koppenhoefer, K. C. and Shih, C. F., 1993, "Effect of Constraint on Specimen Dimensions Needed to Obtain Structurally Relevant Toughness Measures," *Constraint Effects in Fracture*, ASTM STP 1171, pp. 79~103.

Leevers, P. S. and Radon, J. C., 1982, "Inherent Stress Biaxiality in Various Fracture Specimen Geometries," *Int. J. of Fracture*, Vol. 19, pp. 311~325.

McMeeking, R. M. and Parks, D. M., 1989, "Numerical Calculations for Problems of Ductile Fracture," *Advances in Fracture Research*, Vol. 3, pp. 1971~1998.

O'Dowd, N. P. and Shih, C. F., 1991, "Family of Crack-Tip Fields Characterized by a Triaxiality Parameter-I : Structure of Fields," *J. of the Mechanics and Physics of Solids*, Vol. 39, No. 8, pp. 989~1015.

O'Dowd, N. P. and Shih, C. F., 1992, "Family of Crack-Tip Fields Characterized by a Triaxiality Parameter-II : Fracture Applications," *J. of the Mechanics and Physics of Solids*, Vol. 40, No. 5, pp. 939~963.

O'Dowd, N. P. and Shih, C. F., 1992, "Two-Parameter Fracture Mechanics : Theory and Applications," *ASTM 24th National Symposium on Fracture Mechanics*.

O'Dowd, N. P. Shih, C. F. and Dodds, R. H. Jr., 1995, "The Role of Geometry and Crack Growth on Constraint and Implications for Ductile/Brittle Fracture," *Constraint Effects in Fracture*, ASTM STP 1244, pp. 134~159.

Pavankumar, T. V., Seidenfuss, M., Eisele, U. and Roos, E., 2001, "Investigation of Crack-tip Constraint Conditions in Precracked Charpy and Compact Tension Specimens," MPA internal report.

Rice, J. R. and Rosengren, G. F., 1968, "Plane Strain Deformation near a Crack Tip in a Power-Law Hardening Material," *J. of Mechanics and Physics of Solids*, Vol. 16, pp. 1~12.

Shih, C. F., O'Dowd, N. P. and Kirk, M. T., 1991, "A Framework for Quantifying Crack Tip Constraint," *ASTM Symposium on Constraint Effects in Fracture*, Indianapolis.

Sumpter, J. D. G., 1993, "An Experimental Investigation of the T Stress Approach," *Constraint Effects in Fracture*, ASTM STP 1171, pp. 492~502.

Varias, A. G., Suo, Z. and Shih, C. F., 1991, "Ductile Failure of A Constrained Metal Foil," *J. of the Mechanics and Physics of Solids*, Vol. 39, No. 7, pp. 963~986.

Williams, M. L., 1957, "On the Stress Distribution at the Base of a Stationary Crack," *J. of Applied Mechanics*, Vol. 24, pp. 109~114.